Flexible polarization rotation at the ferroelectric/metal interface as a seed for domain nucleation

Xian-Kui Wei, Yurong Yang, Leo J. McGilly, Ludwig Feigl, Rafal E. Dunin-Borkowski, Chun-Lin Jia, Laurent Bellaiche, and Nava Setter

Phys. Rev. B **98**, 020102 — Published 27 July 2018

DOI: 10.1103/PhysRevB.98.020102

Flexible Polarization Rotation at Ferroelectric-Metal Interface as Seed for Domain Nucleation

Xian-Kui Wei,[1,2*] Yurong Yang,[3] Leo J. McGilly,[1] Ludwig Feigl,[1,4] Rafal E. Dunin-Borkowski,[1] Chun-Lin Jia,[2,5] Laurent Bellaiche,[3*] and Nava Setter[1,6]

[1]*Ceramics Laboratory, EPFL-Swiss Federal Institute of Technology, Lausanne 1015, Switzerland*

[2]*Ernst Ruska-Centre for Microscopy and Spectroscopy with Electrons and Peter Grünberg Institute, Forschungszentrum Jülich GmbH, 52425 Jülich, Germany*

[3]*Physics Department and Institute for Nanoscience and Engineering, University of Arkansas, Fayetteville 72701, USA*

[4]*Institute for Photon Science and Synchrotron Radiation, KIT - Karlsruhe Institute of Technology, Hermann-von-Helmholtz-Platz 1,76344 Eggenstein-Leopoldshafen, Germany*

[5]*School of Microelectronics, Xi'an Jiaotong University, Xi'an 710049, China*

[6]*Department of Materials Science and Engineering, Tel-Aviv University, Ramat Aviv 69978, Israel*

*Corresponding author. x.wei@fz-juelich.de & laurent@uark.edu

Abstract:

Missing of the polarization screening scenario at the pivotal ferroelectric-metal interface impedes widespread application of low-dimensional ferroelectric heterostructures. Employing quantitative atom-resolved (scanning) transmission electron microscopy and first-principles calculations, we report that structural and chemical reconstruction universally lowers symmetry of the ferroelectric-metal interface. Irrelevant to structural and strain mismatch, chemical termination and diffusion, polar catastrophe and electrode types, the polarization screening is executed by flexible polarization rotation at the several-unit-cell-thick interfaces. By combining nanoscale and atomic-scale microscopy investigation, our *ex-situ* electric-field biasing experiments reveal that the monoclinically distorted interfaces may play as seeds to nucleate new domains during the polarization switching process. These findings suggest that the long-standing fatigue issue is expected to be overcome by interface modification engineering at monolayer scale.

PACS: 68.37.-d, 68.37.Og, 77.22.Ej, 31.15.A-

Ferroelectric materials are promising candidates to serve as commercial memories because of their faster accessing time, lower energy consumption and potentially lower cost. Recently, the realization of ultrahigh-density ferroelectric nanocapacitor arrays [1,2], at the Tbit inch^{-2} level, makes this aim much closer to practical application. However, its implementation is impeded by long-standing issues such as fatigue [3-5], retention loss and imprint [6,7] during cyclical switching events. These critical issues affect almost all ferroelectric-based memories, including ferroelectric tunnel junctions [8] and ferroelectric-ferromagnetic heterostructures [9]. A particularly important reason lies in the so-called depolarization field [10], which arises from incomplete screening of spontaneous polarization (P_S) at ferroelectric-metal interfaces.

Based on precise control of the interface structure [11,12] and first-principles calculations [13-15], more and more studies point out that clarifying the interfacial screening mechanism is the key to resolve the above issues. However, complicated by factors like structural mismatch, chemical diffusion and charge discontinuity, first-principles calculations and phenomenological Landau-Ginzburg-Devonshire theory [16] fail to depict a complete screening scenario at the unit-cell-scale thick interface. This is evidenced by discrepancy of their screening scenarios from the experimental findings [17-19]. Recently, the compensation phenomena have been explored using aberration-corrected scanning transmission electron microscopy (STEM) [20-22]. Nevertheless, imperfections of the imaging mode [23,24], e.g., unavoidable scanning distortion and weak contrast imaging of oxygen, undermine its capability of performing precise structure investigation at such interfaces.

In this work, we investigate the screening mechanism at a variety of ferroelectric/metal interfaces, e.g., $Pb(Zr_{1-x}Ti_x)O_3$ (PZT)/$SrRuO_3$, $BiFeO_3$/$SrRuO_3$ and Au/PZT, using state-of-the-art microscopy characterization techniques. On the basis of quantitative atom-resolved (S)TEM

studies [25-27] and first-principles calculations, we report that regardless of structural and strain mismatch, chemical termination, polarization orientation and polar catastrophe, the polarization screening is executed by monoclinic distortion enabled flexible polarization rotation at the ferroelectric-metal interfaces. *Ex-situ* electric-field biasing experiments corroborate that the reconstructed interfaces are responsible for nucleation of new domains during the polarization switching process.

Spontaneous polarization (P_S) in perovskite ferroelectrics (ABO_3) is manifested by an overall shift of the polar oxygen octahedral (BO_6) unit with respect to body center of the A-site cationic frame. Taking tetragonal (T) PZT (space group *P4mm*) as an example, its polarization is comprised of uniaxial polar displacements between Zr/Ti and Pb atoms ($\delta z_{Zr/Ti\text{-}Pb}$), O2 and Zr/Ti atoms ($\delta z_{O2\text{-}Zr/Ti}$) and O1 and Pb atoms ($\delta z_{O1\text{-}Pb}$) along the $[001]_T$ direction [Fig. 1(a)]. For oxide electrodes, e.g., orthorhombic (O) $SrRuO_3$ (space group *Pbnm*) [Fig. 1(b)], its structure is featured by antiphase and in-phase rotations of the oxygen octahedra along the orthogonal $[101]_O$, $[10\bar{1}]_O$ axes and along the $[010]_O$ axis, i.e., $a^-a^-c^+$ in Glazer's notation [28]. For typical Au and Pt electrodes, both of them have face-centered cubic structures (space group $Fm\bar{3}m$). At the ferroelectric-metal interfaces, their structures are always complicated by effects of oxygen-octahedral rotation mismatch, chemical termination and diffusion, polar catastrophe and so on [11,20,21].

As the PZT film is grown on a $DyScO_3$ substrates, tensile strain (~ 0.9%) leads to formation of ferroelastic *c/a/c/a* domain array [29] (see **Supplementary Material Fig. S1** [30]). In order to unravel details of these mismatches, $[1\bar{1}0]_T$//$[010]_O$ orientated (x = 0.9) PZT/$SrRuO_3$ specimens are prepared for the TEM study. Figure 1(c) shows an atomically-resolved TEM image of a PZT/$SrRuO_3$ interface. As evidenced by the simulated image [the inset in Fig. 1(c)],

all atomic columns are clearly resolved, in which the Pb-O1 shows single column of Pb/O1 due to their small interatomic separation and exhibits weak contrast at this sample thickness (~5.4 nm). The vertical shifts of oxygen columns (red circles) in opposite directions with respect to

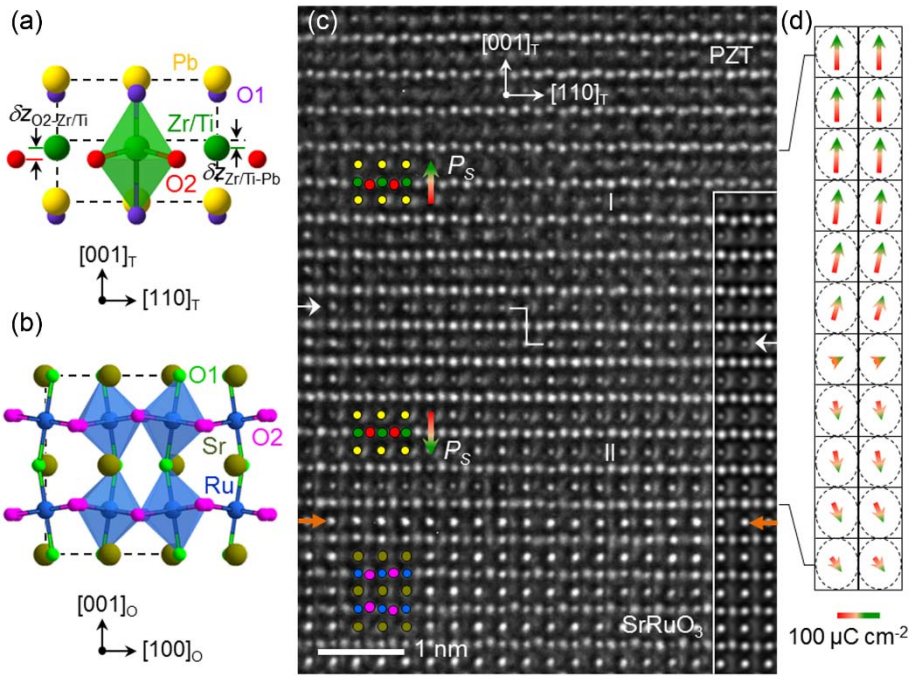

FIG. 1 (single column). (a) Crystal structure of tetragonal PZT with an oxygen-octahedral rotation angle $\phi = 0$ viewed along $[1\bar{1}0]_T$ direction. (b) Crystal structure of orthorhombic $SrRuO_3$ with an oxygen-octahedral rotation angle $\phi \approx 6°$ viewed along $[100]_O$ direction. (c) Atom-resolved TEM image of $DyScO_3$-substrated (x = 0.9) PZT/$SrRuO_3$ interface along the $[1\bar{1}0]_T//[010]_O$ direction recorded under negative spherical-aberration imaging (NCSI) condition. Orange arrows mark the SrO-Zr/TiO_2 terminated interface, white arrows and polygonal line mark the geometric plane of the CDWs. The inset at the lower right shows a simulated image with thickness of 5.4 nm and defocus of 6.0 nm. Atomic column types: Pb/O1-yellow, Zr/Ti-green, O2-red in PZT; Sr/O1-dark yellow, Ru-blue, O2-pink in $SrRuO_3$. (d) Local two-dimensional polarization vectors determined from the structure model used for the image simulation.

neighboring Zr/Ti columns (green circles) mark two domains in this image area: domain I with larger downward shifts of O2 and domain II with smaller upward shifts. These two domains form a tail-to-tail 180° charged domain wall (CDW) with the wall planes normal to the polarization directions and bridged by a unit-cell step in the middle region. Below domain II, the brighter atom columns well define that the interface is terminated by SrO-Zr/TiO_2 atomic planes. Furthermore, buckling of the O2-Ru-O2 atomic planes clearly displays the in-phase octahedral rotation of $SrRuO_3$ along the $[010]_O$ direction.

In order to unravel the polarization compensation mechanism, image-simulation based quantitative TEM study was performed to determine the atomic positions near the interface and the CDW [41]. By removing artifacts affecting the intensity peak positions in the experimental image, e.g., specimen tilting away from the Laue orientation, residual lens aberrations and the interfacial element diffusion (see **Supplementary Material Fig. S2** [30]), measurement of the individual atomic shift at picometer precision becomes accessible.

Figure 2(a) shows the lattice parameter changes as a function of distance normal to the interface. Compared with the nearly constant pseudocubic (p) a_p-axis ($a_p = \sqrt{2}a_O/2$ for $SrRuO_3$ and $a_p \approx a_T$ for PZT), ~0.3913 nm, pronounced changes are observed along the c-axis direction. Via a smooth reduction in domain I (c = 0.4160 nm, c/a = 1.063), the c axis measured from Pb atoms (blue squares) steeply increases to 0.4246 nm (c/a = 1.085) near the CDW. A stepwise decrease is then observed in the middle of domain II ($c/a \approx$ 1.042) and near the interface (c/a = 1.025). The c axes measured from Zr/Ti atoms (pink squares) show smaller values, which diverge from the larger values determined from the Pb atoms. On the $SrRuO_3$ side, nevertheless, a reversed tendency ($c_{p\text{-Sr}} < c_{p\text{-Ru}}$) is observed in ~3 pseudocubic unit cells near the interface.

These divergent behaviors, reflecting rearrangement of atomic positions inside the unit cells, can be attributed to lattice responses to polarization screening at both interfaces. For the horizontal O2-Ru-O2 atomic planes of $SrRuO_3$ [Fig. 1(c)], the in-phase octahedral rotation results in alternate up and down shifts of O2 atoms around the Ru positions. As approaching the interface, the displacements decrease in magnitude and penetrate into the PZT layer by 2 unit cells [Fig. 2(b)]. Meanwhile, the polar displacements of O2 atoms ($\delta z_{O2\text{-}Zr/Ti}$) in PZT also propagate into the $SrRuO_3$ electrode by 1 ~ 2 pseudocubic unit cells. As a result of interface bonding [13,42] and polarization screening, the antiferrodistortive order then couples with the ferroelectric order at the reconstructed interface, which is further evidenced by polar displacements of Ru atoms ($\delta z_{Ru\text{-}Sr}$) near the interface [inset in Fig. 2(b)]. Another interesting point worth noting is the antiparallel displacements between Zr/Ti and O2 atoms in the two longest unit cells near the CDW. This local violation of the crystallographic symmetry can be attributed to inequivalent polarization between domain-I (P_{SZ} = 84 μC cm^{-2}) and domain-II (P_{SZ} = -45 μC cm^{-2}) [Fig. 2(c)]. The P_{SZ} profile indicates that width of the CDW is 6 unit cells, and the polarization extrapolates 1~2 pseudocubic unit cells into the $SrRuO_3$ [**see Supplementary Material** [30]].

More unexpected findings are revealed by the in-plane atomic displacements [Figs. 2(d), 2(e)]. At the PZT/$SrRuO_3$ interface, polar displacements of the B-site ($\delta x_{B\text{-}A} \approx$ -5 pm) and O2 ($\delta x_{O2\text{-}B} \approx$ -7.5 pm) atoms clearly show that the interfacial unit cells are monoclinically distorted [43]. Calculation yields that the in-plane polarization is $P_{SX} \approx$ 23.6 μC cm^{-2} and width of the polarized interface is ~6 unit cells [Fig. 2(f)]. Near the CDW, the Zr/Ti atoms undergo large displacements with $\delta x_{Zr/Ti\text{-}Pb} \approx$ -20 pm at the wall plane. However, the relative displacements between O2 and Zr/Ti atoms are absent. Assuming that the separation takes place between

positively charged Pb^{2+} cations and negatively charged $(Zr/TiO_6)^{2-}$ octahedra [44], an in-plane polarization with P_{SX} = 17 μC cm^{-2} is developed inside the monoclinically distorted lattices, which is supported by first-principles calculations of CDWs on $PbTiO_3$ [45].

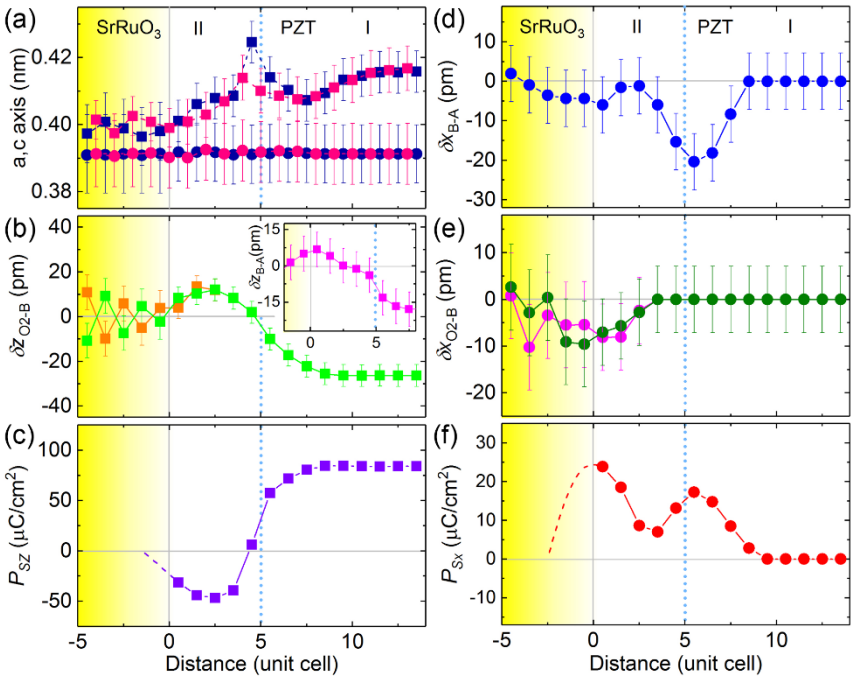

FIG. 2 (single column). (a) The *c* (squares) and *a* (circles) axes measured from A-site (blue) and B-site (red) atoms, respectively. (b) Out-of-plane displacements of O2 atoms ($\delta z_{O2\text{-}B}$) and (inset) B-site atoms ($\delta z_{B\text{-}A}$). (c) Out-of-plane polarization (P_{SZ}) extrapolated into the $SrRuO_3$ (purple dashed line). (d),(e) In-plane displacements of B-site ($\delta x_{B\text{-}A}$) and O2 ($\delta x_{O2\text{-}B}$) atoms, respectively. (f) In-plane polarization (P_{SX}) extrapolated into the $SrRuO_3$ (red dashed line). These profiles are plotted as a function of distance normal to the interface. The blue dotted lines mark position of the CDW. The yellow shadow denotes reduced electron density of $SrRuO_3$ in terms of decreased rotation of oxygen octahedra towards the interface.

To quantify the interfacial chemical diffusion, atomic-resolution energy-dispersive X-ray spectroscopy (EDS) was performed on the (x = 0.9) PZT/$SrRuO_3$ interface areas [Fig. 3(a)]. For

A-site elements, the Sr atom is found to diffuse strongly into the PZT layer over one atomic layer [Figs. 3(b), 3(c)]. While for B-site elements, the Ti atom reversely diffuses into the $SrRuO_3$ electrode over one atomic layer [Figs. 3(d), 3(e)]. The elemental profiles reveal the asymmetric chemical diffusion and the SrO-Zr/TiO_2-plane terminated interface [Figs. 3(f)]. The composition of the first interfacial unit cell is approximately $(Pb_{0.4}Sr_{0.6})(Zr_{0.1}Ti_{0.7}Ru_{0.2})O_3$ on the PZT side and $(Sr_{0.75}Pb_{0.25})(Ru_{0.5}Ti_{0.5})O_3$ on the $SrRuO_3$ side.

These results highlight that driven by structural and chemical reconstruction, the SrO-Zr/TiO_2 terminated PZT/$SrRuO_3$ interface is characteristic of monoclinic lattice distortion and flexible polarization rotation. Specifically, the incorporation of Sr into the PZT layer [46,47] reduces the interfacial lattice tetragonality and the magnitude of P_{SZ}. At the same time, metal-to-insulator transition, which takes place at x = 0.5 in $Sr(Ru_{1-x}Ti_x)O_3$ [48], suppresses the interface conductivity and results in penetration of polarization into the $SrRuO_3$ electrode. Together with the structural reconstruction, the monoclinic lattice distortion therefore facilitates the development of in-plane polarization at the interface.

This screening scenario is supported by our first-principles calculations on Sr and Ru co-doped $PbTiO_3$ and a report of polarized SrO planes at $SrRuO_3/BaTiO_3$ interfaces [49]. By averaging the composition of the second-to-fourth unit cells in domain II, a supercell of $(Pb_{0.75}Sr_{0.25})(Ti_{0.75}Ru_{0.25})O_3$ was constructed for the calculation [see **Supplementary Material Fig. S3** [30]]. Our result shows that the supercell with monoclinic symmetry (space group *Cm*) has the lowest energy and the polarization is allowed to rotate freely within the confined $(1\bar{1}0)_T$ plane. By fixing the in-plane lattice constant to bulk value of $SrRuO_3$, the out-of-plane and in-plane polarizations are P_{SZ} = 66.2 μC cm^{-2} and P_{SX} = 13.2 μC cm^{-2} for the supercell, which are close to the experimental values presented in Figs. 2(c) and 2(f). Meanwhile, the inert

displacements of Ru atoms along $[001]_T$ direction manifest their passive contribution to polarization penetration into the $SrRuO_3$ electrode [Fig. 3(g)]. Apart from the ionic screening, the decreased oxygen octahedral rotation [50,51] also provides evidence for impaired electronic screening as approaching the interface, which is denoted by yellow shadow in Fig. 2. Therefore, an "*in-situ*" screening scenario is suggested at the oxide heterointerface [13-15].

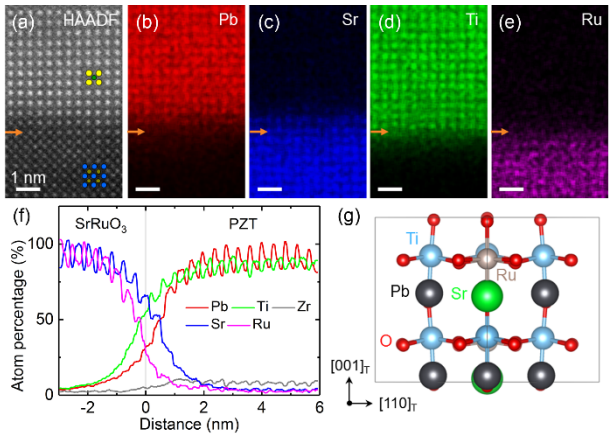

FIG. 3 (single column). (a) Atomically-resolved high-angle annular-dark-field (HAADF)-STEM image of the (x = 0.9) PZT/$SrRuO_3$ interface (orange arrows) recorded along $[100]_T$ direction. Atomic column types: Pb-yellow, Zr/Ti-green, Sr-dark yellow, Ru-blue. (b)-(e) EDS maps for Pb, Sr, Ti and Ru, respectively. (f) Averaged atomic percentage profiles for the heavy atoms across the SrO-Zr/TiO_2 terminated interface. (g) First-principles calculated $(Pb_{0.75}Sr_{0.25})(Ti_{0.75}Ru_{0.25})O_3$ supercell (space group *Cm*) viewed along $[1\bar{1}0]_T$ direction.

In order to verify validity and universality of the screening mechanism, a more complex $BiFeO_3/SrRuO_3$ interface, involving polar catastrophe, oxygen-octahedral rotation mismatch, strain mismatch and chemical diffusion, was examined by HAADF-STEM [**Supplementary Material, Fig. S4** [30]]. In the $BiFeO_3$ layer, the lower-left and upper-left displacements of Fe clearly identify a tail-to-tail 71° or 109° CDW with the domain polarization pointing along the

projected <011>$_p$ direction [Fig. 4(a)]. Similarly, the epitaxial growth relationship yields a constant a_p axis (~ 0.3980 nm) and the CDW leads to lattice expansion ($c/a \approx 1.042$) with respect to the domains ($c/a \approx 1.024$) [Fig. 4(b)]. Nevertheless, the c_p axis is found to reduce abruptly from 0.4209 nm ($c/a \approx 1.057$) to 0.3926 nm ($c/a \approx 0.986$) as passing across the interface, which is accompanied with a decrease/increase in out-of-plane/in-plane displacement ($\delta z_{\text{Fe-Bi}}/\delta x_{\text{Fe-Bi}}$) on the $BiFeO_3$ side, and dominance of the in-plane displacements ($\delta z_{\text{Ru-Sr}} \approx 8.9$ pm) on the $SrRuO_3$ side [Fig. 4(c)]. These structural changes provide evidence for a monoclinic-like lattice distortion at the $BiFeO_3/SrRuO_3$ interface (~ 6 unit-cell thick) and the CDW, thereby enabling the polarization to rotate flexibly within the symmetry-permitted planes [Fig. 4(a)].

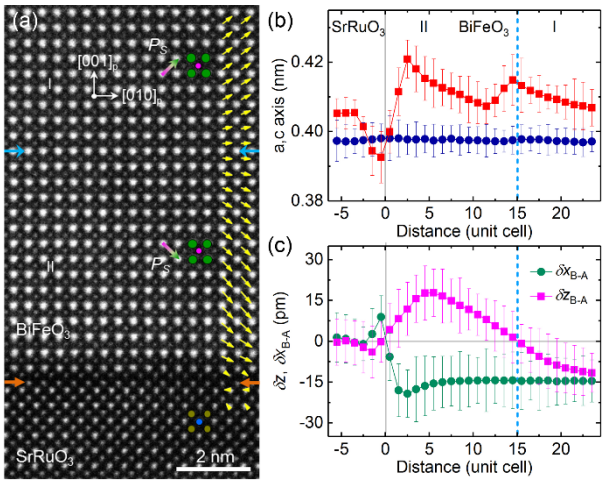

FIG. 4 (single column). (a) Atom-resolved HAADF-STEM image of $BiFeO_3/SrRuO_3$ interface, involving polar catastrophe, oxygen-octahedral rotation mismatch ($\phi \approx 12°$ for $BiFeO_3$ and $\phi \approx 6°$ for $SrRuO_3$) and chemical diffusion, recorded along $[100]_p$ direction. The yellow, orange and blue arrows denote the polar displacement vectors compiled from (c), SrO-FeO_2 termination and CDW, respectively. Atomic column types: Bi-green, Fe-pink, Sr-dark yellow, Ru-blue. (b),(c) Lattice parameter and polar displacement changes measured across the interface and the CDW (blue dashed lines) and plotted as a function of distance normal to the interface.

Apart from the SrO-BO_2 termination, the PZT/$SrRuO_3$ interfaces terminated by RuO_2-PbO atomic planes were also investigated [**Supplementary Material, Fig. S5** [30]]. The impact of interface termination type on internal built-in field is discussed with respect to the measured hysteresis loops [**Supplementary Material, Fig. S6** [30]]. In contrast to the SrO-BO_2 termination, the RuO_2-PbO termination results in a downward orientation of P_S (towards the interface) in the entire *c* domains. According to density functional theory calculation [52], the worse/better screening capability of $SrRuO_3$ electrode with SrO/RuO_2 termination may therefore explain presence/absence of the interfacial CDWs inside the *c* domains [30]. More importantly, the interface reconstruction enabled flexible polarization rotation is also verified at the RuO_2-PbO terminated interfaces, which is also irrelevant to change of the oxygen partial pressure (0.1 ~ 1 mbar) during sample growth [**Supplementary Material, Fig. S7** [30]]. In analogy to oxide electrodes, Au and Pt electrodes also lead to flexible polarization rotation at metal-electrode/PZT interfaces, which are about 3 unit cells [**Supplementary Material, Fig. S8** [30]]. The observed universality of the screening mechanism suggests that the ferroelectric-metal interfaces may act as seeds to nucleate new domains during the polarization switching process. Considering the distinct switching dynamics of ferroelastic domains [53,54], the model system Pt/PZT/$SrRuO_3$/$SrTiO_3$, with mono-domain ferroelectric state, was selected to confirm this argument by means of *ex-situ* biasing and TEM/STEM investigations [**Supplementary Material, Fig. S9** [30]].

By switching the Pt-electrode covered regions, an array of 180° domains, with the DWs lying in the $(100)_T$ plane, was achieved in the Pt patterned square area [Figs. 5(a) and 5(b)]. A non-uniform piezoresponse force microscopy (PFM) phase image suggests that the polarization

in the targeted regions was not fully switched. Manifested by bright-contrast spots, cross-sectional dark-field TEM imaging shows that the incomplete domain switching leads to preferential nucleation of nano-domains (diameter at 3 ~ 14 nm) near the PZT/$SrRuO_3$ and Pt/PZT interfaces [Fig. 5(c)]. This is confirmed by atom-resolved HAADF-STEM observations on the written DW area. The newly created nano-domains near the interfaces, which are surrounded by the initial-state domain with an upward P_S orientation, are found to possess reversed P_S orientation along with in-plane atomic displacements [Fig. 5(d)]. This result confirms that the low-symmetric ferroelectric-metal interfaces indeed induce nucleation of new domains during the polarization switching process.

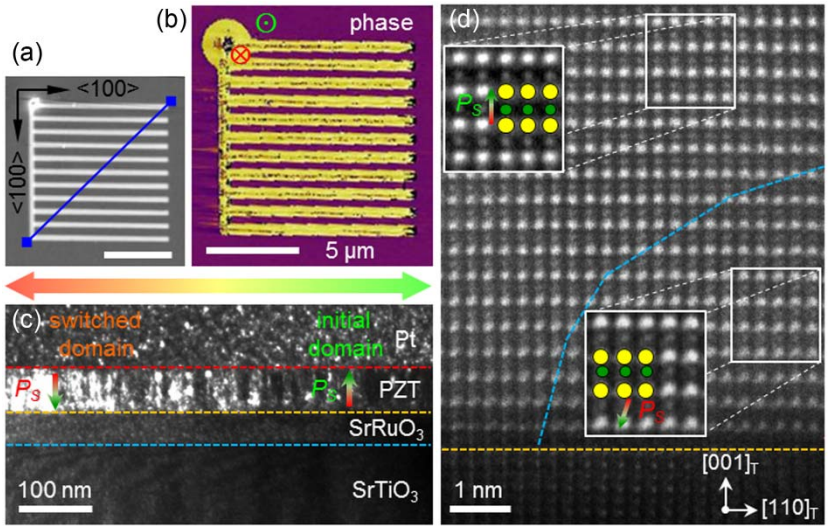

FIG. 5 (single column). *Ex-situ* electric-field biasing and microscopy characterization of x = 0.6 PZT film. (a) Topography image of patterned Pt top electrode. The blue line denotes location of the cross-sectional FIB lamella. (b) PFM phase image of the entire area after switching the Pt-covered regions by +8 V voltage pulse (⊙-upward and ⊗-downward P_S orientations). (c) Dark-field TEM image of the written domain boundary recorded under two-beam conditions using **g** = $(00\bar{2})$ reflection. The color dashed lines mark the interfaces. (d) Corresponding atom-resolved HAADF-STEM image recorded along the $[1\bar{1}0]_T$ direction. The blue dashed line delineates the

boundary between the initial and newly nucleated domains. The insets are filtered to highlight the atomic details (Pb/O1-yellow circles, Zr/Ti-green circles).

The seed effect of the ferroelectric-metal interface is further supported by the observation of polarization curling and flux closure structures in multiferroic Co/$PbTiO_3$/(La,Sr)MnO_3 tunnel junctions [55], in which flexible polarization rotation is identified near both interfaces. Since the in-plane polarization component does not contribute to the interface capacitance, it therefore plays a deleterious role in practical ferroelectric devices [56]. In addition, photoemission and X-ray absorption study reveals that Ti remains tetravalent in the $Sr(Ru_{1-x}Ti_x)O_3$ ($0 \leq x \leq 1$) films [57], suggesting that oxygen vacancies, which may be generated in the operating devices, are not necessary ingredient for compensation of ferroelectric polarization at the initial-state interfaces.

In fact, the screening scenario deciphered at the ferroelectric-metal heterointerfaces is analogous to the behavior at interfacial CDWs. Driven by polarization discontinuity, monoclinic-like lattice distortion associated with atomic rearrangement enables development of the in-plane polarization. As a result, flexible polarization rotation leads to cycloidal polarization configuration at the CDWs [Figs. 1(d) and 4(c)], which is different from the reported charged 180° and 90° DWs in $PbTiO_3$ films [41,58] and charged 71°, 109° and 180° DWs in $BiFeO_3$ films [59]. Consideration of the electrostatic energy indicates that the in-plane polarizations at the interface and the CDW are independent on each other [43], as Néel-like DW configuration would otherwise be favored between the interfacial areas.

In summary, driven by structural and chemical mismatches, the reconstructed ferroelectric-metal interfaces break the parent lattice symmetries and universally adopt low-symmetry monoclinic structures [60-62]. As a consequence, the polarization screening is

implemented by flexible polarization rotation at the reconstructed interfaces, which are responsible for nucleation of new domains during the polarization switching process. In order to overcome degradation of the ferroelectric devices [3], our findings suggest that interface engineering, e.g., conductivity modification by inserting alien atomic monolayer [63,64], is expected to revive screening effectiveness of the electrodes. It is hoped that such measures may overcome the long-standing fatigue issue and that application of ferroelectric-based devices will become widespread in the future.

Acknowledgements

The research leading to these results has received funding from the European Research Council under the EU 7th Framework Programme (FP7/2007-2013) / ERC grant agreement n◦ [268058] Mobile-W and from the EU 7th Framework Programme under Grant Agreement 312483 - ESTEEM2 (Integrated Infrastructure Initiative–I3). Y.Y. and L.B. acknowledge the ONR Grant N00014-12-1-1034 and N00014-17-1-2818. The authors thank M. Kruth and D. Meertens for sample preparation using focused ion beam.

References

[1] W. Lee, H. Han, A. Lotnyk, M. A. Schubert, S. Senz, M. Alexe, D. Hesse, S. Baik, and U. Gosele, Nat. Nanotechnol. **3**, 402 (2008).

[2] Y. Cho, S. Hashimoto, N. Odagawa, K. Tanaka, and Y. Hiranaga, Nanotechnology **17**, S137 (2006).

[3] A. K. Tagantsev, I. Stolichnov, E. L. Colla, and N. Setter, J. Appl. Phys. **90**, 1387 (2001).

[4] D.-H. Do, P. G. Evans, E. D. Isaacs, D. M. Kim, C. B. Eom, and E. M. Dufresne, Nat. Mater. **3**, 365 (2004).

[5] X. Zou, L. You, W. G. Chen, H. Ding, D. Wu, T. Wu, L. Chen, and J. Wang, ACS Nano **6**, 8997 (2012).

[6] Y.-H. Hsieh, F. Xue, T. Yang, H.-J. Liu, Y. Zhu, Y.-C. Chen, Q. Zhan, C.-G. Duan, L.-Q. Chen, Q. He, and Y.-H. Chu, Nat. Commun. **7**, 13199 (2016).

[7] Y. Zhou, H. K. Chan, C. H. Lam, and F. G. Shin, J. Appl. Phys. **98**, 024111 (2005).

[8] V. Garcia and M. Bibes, Nat. Commun. **5**, 4289 (2014).

[9] J. M. Hu, L. Q. Chen, and C. W. Nan, Adv. Mater. **28**, 15 (2016).

[10] D. J. Kim, J. Y. Jo, Y. S. Kim, Y. J. Chang, J. S. Lee, J.-G. Yoon, T. K. Song, and T. W. Noh, Phys. Rev. Lett. **95**, 237602 (2005).

[11] P. Yu, W. Luo, D. Yi, J. X. Zhang, M. D. Rossell, C. H. Yang, L. You, G. Singh-Bhalla, S. Y. Yang, Q. He, Q. M. Ramasse, R. Erni, L. W. Martin, Y. H. Chu, S. T. Pantelides, S. J. Pennycook, and R. Ramesh, Proc. Natl. Acad. Sci. U. S. A. **109**, 9710 (2012).

[12] Y. J. Shin, Y. Kim, S. J. Kang, H. H. Nahm, P. Murugavel, J. R. Kim, M. R. Cho, L. Wang, S. M. Yang, J. G. Yoon, J. S. Chung, M. Kim, H. Zhou, S. H. Chang, and T. W. Noh, Adv. Mater. **29**, 1602795 (2017).

[13] N. Sai, A. M. Kolpak, and A. M. Rappe, Phys. Rev. B **72**, 020101(R) (2005).

[14] G. Gerra, A. K. Tagantsev, N. Setter, and K. Parlinski, Phys. Rev. Lett. **96**, 107603 (2006).

[15] M. Stengel, D. Vanderbilt, and N. A. Spaldin, Nat. Mater. **8**, 392 (2009).

[16] A. N. Morozovska, E. A. Eliseev, S. V. Svechnikov, A. D. Krutov, V. Y. Shur, A. Y. Borisevich, P. Maksymovych, and S. V. Kalinin, Phys. Rev. B **81**, 205308 (2010).

[17] C. S. Hwang, J. Appl. Phys. **92**, 432 (2002).

[18] D. P. Vijay and S. B. Desu, J. Electrochem. Soc. **140**, 2640 (1993).

[19] F. Chen and A. Klein, Phys. Rev. B **86**, 094105 (2012).

[20] M. F. Chisholm, W. Luo, M. P. Oxley, S. T. Pantelides, and H. N. Lee, Phys. Rev. Lett. **105**, 197602 (2010).

[21] S.-B. Mi, C.-L. Jia, I. Vrejoiu, M. Alexe, and D. Hesse, Adv. Mater. Interfaces **2**, 1500087 (2015).

[22] Y. M. Kim, A. Morozovska, E. Eliseev, M. P. Oxley, R. Mishra, S. M. Selbach, T. Grande, S. T. Pantelides, S. V. Kalinin and A. Y. Borisevich, Nat. Mater. **13**, 1019 (2014).

[23] F. F. Krause, M. Schowalter, T. Grieb, K. Muller-Caspary, T. Mehrtens, and A. Rosenauer, Ultramicroscopy **161**, 146 (2016).

[24] Y. G. So and K. Kimoto, J. Electron Microsc. **61**, 207 (2012).

[25] C. L. Jia, M. Lentzen, and U. K., Science **299**, 870 (2003).

[26] K. W. Urban, C. L. Jia, L. Houben, M. Lentzen, S. B. Mi, and K. Tillmann, Phil. Trans. A Math. Phys. Eng. Sci. **367**, 3735 (2009).

[27] C. L. Jia, L. Houben, A. Thust, and J. Barthel, Ultramicroscopy **110**, 500 (2010).

[28] A. T. Zayak, X. Huang, J. B. Neaton, and K. M. Rabe, Phys. Rev. B **74**, 094104 (2006).

[29] X. K. Wei, T. Sluka, B. Fraygola, L. Feigl, H. Du, L. Jin, C. L. Jia, and N. Setter, ACS Appl. Mater. Interfaces **9**, 6539 (2017).

[30] See Supplemental Material for details on experimental methods, domain configurations, surface and interface information for the (x = 0.9, 0.6) PZT and $BiFeO_3$ films, quantitative atom-resolved (S)TEM studies, identification of interface termination, first-principles calculations, effects of polar catastrophe, RuO_2-PbO termination, oxygen partial pressure, polarization orientation and strain mismatch on polarization screening, effect of interface termination on

internal built-in field, and implementation of *ex-situ* biasing experiments, which includes Refs. [31-40].

[31] L. Feigl, P. Yudin, I. Stolichnov, T. Sluka, K. Shapovalov, M. Mtebwa, C. S. Sandu, X. K. Wei, A. K. Tagantsev, and N. Setter, Nat. Commun. **5**, 4677 (2014).

[32] I. Stolichnov, M. Iwanowska, E. Colla, B. Ziegler, I. Gaponenko, P. Paruch, M. Huijben, G. Rijnders, and N. Setter, Appl. Phys. Lett. **104**, 132902 (2014).

[33] W. Zhong, R. D. King-Smith, and D. Vanderbilt, Phys. Rev. Lett. **72**, 3618 (1994).

[34] P. D. Nellist and S. J. Pennycook, Adv. Imag. Elect. Phys. **113**, 147 (2000).

[35] G. Kresse and J. Furthmuller, Phys. Rev. B **54**, 11169 (1996).

[36] G. Kresse and D. Joubert, Phys. Rev. B **59**, 1758 (1999).

[37] O. Grånäs, I. Di Marco, O. Eriksson, L. Nordström, and C. Etz, Phys. Rev. B **90**, 165130 (2014).

[38] S. V. Kalinin, A. Borisevich, and D. Fong, ACS Nano **6**, 10423 (2012).

[39] L. Feigl, P. E. Janolin, T. Yamada, M. Iwanowska, C. S. Sandu, and N. Setter, Appl. Phys. Lett. **106**, 032902 (2015).

[40] M. J. Highland, T. T. Fister, D. D. Fong, P. H. Fuoss, C. Thompson, J. A. Eastman, S. K. Streiffer, and G. B. Stephenson, Phys. Rev. Lett. **107**, 187602 (2011).

[41] C.-L. Jia, S.-B. Mi, K. Urban, I. Vrejoiu, M. Alexe, and D. Hesse, Nat. Mater. **7**, 57 (2007).

[42] M. G. Han, M. S. Marshall, L. Wu, M. A. Schofield, T. Aoki, R. Twesten, J. Hoffman, F. J. Walker, C. H. Ahn, and Y. Zhu, Nat. Commun. **5**, 4693 (2014).

[43] X.-K. Wei, C.-L. Jia, T. Sluka, B.-X. Wang, Z.-G. Ye, and N. Setter, Nat. Commun. **7**, 12385 (2016).

[44] N. Zhang, H. Yokota, A. M. Glazer, Z. Ren, D. A. Keen, D. S. Keeble, P. A. Thomas, and Z. G. Ye, Nat. Commun. **5**, 5231 (2014).

[45] X. Wu and D. Vanderbilt, Phys. Rev. B **73**, 020103(R) (2006).

[46] D. H. Kang, J. H. Kim, J. H. Park, and K. H. Yoon, Mater. Res. Bull. **36**, 265 (2001).

[47] T. Qi, I. Grinberg, and A. M. Rappe, Phys. Rev. B **82**, 134113 (2010).

[48] K. W. Kim, J. S. Lee, T. W. Noh, S. R. Lee, and K. Char, Phys. Rev. B **71**, 125104 (2005).

[49] P. Aguado-Puente, and J. Junquera, Phys. Rev. Lett. **100**, 177601 (2008).

[50] W. Lu, W. Song, P. Yang, J. Ding, G. M. Chow, and J. Chen, Sci. Rep. **5**, 10245 (2015).

[51] R. Gao, Y. Dong, H. Xu, H. Zhou, Y. Yuan, V. Gopalan, C. Gao, D. D. Fong, Z. Chen, Z. Luo, and L. W. Martin, ACS Appl. Mater. Interfaces **8**, 14871 (2016).

[52] S. Divilov and M.-V. Fernandez-Serra, APS March Meeting, 2015APS..MARJ13006D (2015).

[53] P. Gao, J. Britson, J. R. Jokisaari, C. T. Nelson, S. H. Baek, Y. Wang, C. B. Eom, L. Q. Chen, and X. Pan, Nat. Commun. **4**, 2791 (2013).

[54] P. Gao, J. Britson, C. T. Nelson, J. R. Jokisaari, C. Duan, M. Trassin, S. H. Baek, H. Guo, L. Z. Li, Y. R. Wang, Y. H. Chu, A. M. Minor, C. B. Eom, R. Ramesh, L. Q. Chen, X. Q. Pan, Nat. Commun. **5**, 3801 (2014).

[55] J. J. Peters, G. Apachitei, R. Beanland, M. Alexe, and A. M. Sanchez, Nat. Commun. **7**, 13484 (2016).

[56] M. Stengel and N. A. Spaldin, Nature **443**, 679 (2006).

[57] J. Kim, J. Y. Kim, B. G. Park, and S. J. Oh, Phys. Rev. B **73**, 235109 (2006).

[58] Y. L. Tang, Y. L. Zhu, Y. J. Wang, W. Y. Wang, Y. B. Xu, W. J. Ren, Z. D. Zhang, and X. L. Ma, Sci. Rep. **4**, 4115 (2014).

[59] W.-Y. Wang, Y.-L. Tang, Y.-L. Zhu, Y.-B. Xu, Y. Liu, Y.-J. Wang, S. Jagadeesh, and X.-L. Ma, Adv. Mater. Interfaces **2**, 1500024 (2015).

[60] S. R. Spurgeon, P. V. Balachandran, D. M. Kepaptsoglou, A. R. Damodaran, J. Karthik, S. Nejati, L. Jones, H. Ambaye, V. Lauter, Q. M. Ramasse, K. K. Lau, L. W. Martin, J. M. Rondinelli, and M. L. Taheri, Nat. Commun. **6**, 6735 (2015).

[61] A. Y. Borisevich, H. J. Chang, M. Huijben, M. P. Oxley, S. Okamoto, M. K. Niranjan, J. D. Burton, E. Y. Tsymbal, Y. H. Chu, P. Yu, R. Ramesh, S. V. Kalinin, and S. J. Pennycook, Phys. Rev. Lett. **105**, 087204 (2010).

[62] C. Chen, S. Lv, J. Li, Z. Wang, X. Liang, Y. Li, D. Viehland, K. Nakajima, and Y. Ikuhara, Appl. Phys. Lett. **107**, 031601 (2015).

[63] P. Z. Wang, T. Y. Cai, S. Ju, and Y. Z. Wu, Sci. Rep. **6**, 24209 (2016).

[64] D. Stornaiuolo, C. Cantoni, G. M. De Luca, R. Di Capua, E. Di Gennaro, G. Ghiringhelli, B. Jouault, D. Marre, D. Massarotti, F. Miletto Granozio, I. Pallecchi, C. Piamonteze, S. Rusponi, F. Tafuri, and M. Salluzzo, Nat. Mater. **15**, 278 (2016).